Influence of Nb stabilization on the recovery and recrystallization kinetics of a ferritic stainless steel with soft magnetic properties for automotive applications

Influência da estabilização do Nb na cinética de recuperação e recristalização de um aço inoxidável ferrítico com propriedades magnéticas macias para aplicações automotivas

Nicolas Meyer
UGITECH, Schmolz + Bickenbach group
Research Center, Avenue Paul Girod,
73403 Ugine, France
nicolas.meyer@ugitech.com

Marc Mantel
UGITECH, Schmolz + Bickenbach group
Research Center, Avenue Paul Girod,
73403 Ugine, France
marc.mantel@ugitech.com

P.E.Dubois
UGITECH, Schmolz + Bickenbach group
Research Center, Avenue Paul Girod,
73403 Ugine, France
pe.dubois@ugitech.com

Muriel Veron
SIMAP INPGrenoble-CNRS-UJF,
Groupe Physique du Métal,
BP 75, 38402 Saint Martin d'Hères – France
muriel.veron@phelma.grenoble-inp.fr

Yves Brechet
SIMAP INPGrenoble-CNRS-UJF,
Groupe Physique du Métal,
BP 75, 38402 Saint Martin d'Hères – France
yves.brechet@simap.grenoble-inp.fr

Olivier Geoffroy
Laboratoire Louis Néel, CNRS,
BP 166, 38042 Grenoble - France
geoffroy@grenoble.cnrs.fr

Abstract

Usually niobium is added in ferritic stainless steels to avoid chromium carbides precipitation and then to improve corrosion resistance and to avoid embrittlemet. This study shows that a low Nb stabilization makes recrystallization nucleation much faster and prevents incomplete recrystallization. A qualitative interpretation, based on interaction with precipitates, is proposed and explains the main features of the softening kinetics as well as the microstructures obtained. Above a specific magnetizing frequency, the deformed state led to smaller losses than the recrystallized state. These results are believed to be attributed to a grain size effect. This leads to soft magnetic properties that makes 17%CrNb ferritic stainless steels a very interesting solution for the market of electromagnetic injection. Improving response-time of fuel injection valves is a great challenge for automotive industry in order to enhance car engine efficiency and to limit noxious gas emission.

Keywords: Ferritic stainless steel, recrystallysation, magnetic properties, niobium stabilization.

Resumo

Normalmente o nióbio é adicionado aos aços inoxidáveis ferríticos para se evitar a precipitação de carbonetos de cromo e, em seguida, para se melhorar a resistência à corrosão e para se evitar a fragilização. Esse estudo mostra que a estabilização com baixo Nb baixo promove a nucleação da recristalização muito mais rapidamente e evita a recristalização incompleta. Uma interpretação qualitativa, baseada na interação com precipitados, é proposta. Nessa interpretação, explicam-se as principais características da cinética de amolecimento, bem como as microestruturas obtidas. Acima de uma frequência específica de magnetização, o estado deformado leva a perdas menores do que o estado recristalizado. Acredita-se que esses resultados podem ser atribuídos a um efeito de tamanho de grão. Isto leva a propriedades magnéticas macias, que faz dos aços inoxidáveis ferríticos 17% CrNb uma solução muito interessante para o mercado de injeção eletromagnética. Melhorar o tempo de resposta das válvulas de injeção de combustível é um grande desafio da indústria automobilística, a fim de se aumentar a eficiência dos motores, quanto às emissões de gases tóxicos.

Palavras-chave: *Aço inoxidável ferrítico, recristalização, propriedades magnéticas, estabilização pelo nióbio.*

1. Introduction

Improving response-time of fuel injection valves is a great challenge for automotive industry because it constitutes a direct way to enhance car engine efficiency and to limit noxious gas emission. For an electromagnetic injector, the response-time depends particularly on the magnetic properties of the actuator.

17% Cr ferritic stainless steels is a very interesting solution for actuation because it combines a good corrosion resistance with rather soft magnetic properties [Ara]. The aim of the project is to find the optimum adjustment of microstructure to lower magnetic losses under dynamic excitation.

To understand the relationship between microstructure and magnetic losses, different microstructural states have been generated by varying annealing conditions that led to either recovery or to recrystallization. Low level niobium stabilization was also considered in order to widen the range of microstructures formed, since niobium is an important addition element in the design of corrosion resistant stainless steels [Mantel]. This article mainly focuses on the understanding of the annealing phenomena kinetics and the microstructure evolution. Interaction between magnetic losses and microstructure is illustrated on the Nb stabilized grade to demonstrate the interest of such an approach.

2. Materials and experimental procedure

Initial state

Table 1 reports the chemical composition of the two industrial casts melted by UGITECH and considered in this work. The materials were received in the form of wires of diameter 12.5 mm, obtained by hot rod rolling around 1200°C. To start from fully ferritic states for both grades, an additional heat treatment around 850°C was performed on 430 to remove the martensite formed during cooling from 1200°C. In the initial state, both grades are fully ferritic and have the same hardness (HV1 = 145). However, a major difference concerning precipitation is seen on Figure 1: 430Nb exhibits homogeneous precipitation of Nb(C,N) whereas, in 430, the precipitates identified as Cr_2N and $M_{23}C_6$ are located in grain boundaries and in bands parallel to the rolling direction.

Grade (AISI)	C	N	CR	Nb	Mn	Si	DNb
430	0,017	0,028	16,083	0,004	0,405	0,345	-
430Nb	0,015	0,012	16,284	0,27	0,324	0,35	0,076

Table 1
Chemical composition analysis and stabilization level ΔNb [wt. %]; the stoichiometric relation for ΔNb is given in [Mantel].

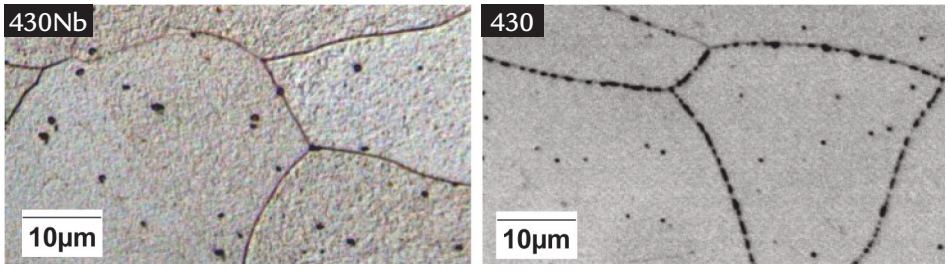

Figure 1
Optical micrographs in the initial state after etching using Villela reagent. 430Nb presents weak homogeneous precipitation whereas 430 exhibits intense intergranular precipitation.

Laboratory thermomechanical treatments

From initial state on, the two grades received exactly the same thermomechanical treatments. First, a 20% nominal strain in tension was performed at room temperature and at $3.10^{-4}s^{-1}$ strain rate. After this cold deformation, heat treatments were performed in a salt bath at two temperatures (750°C and 850°C) for different times from 30 s to 1 h and were followed by quenching in water. The accurate thermal analysis curve at the center of the rod was measured with a thermocouple inserted in a hole drilled along the rod axis and revealed that the salt bath temperature is reached to within 10°C after 40 s. The temperature versus time relationship T(t) has been determined by fit on experimental thermal analysis data but, is not detailed here for conciseness reasons.

Longer heat treatments at 850°C, from 2 h to 16 h, were performed in a resistor furnace under argon atmosphere. In these cases, heating stage will be disregarded compared to isothermal stage.

Characterization

Global softening kinetics were followed by microhardness HV1 in the center of a transverse section of the rod. This softening is the result of two competing phenomena: recovery, which is active from the start of the annealing treatment and recrystallization that begins after an incubation time.

Grain structure was revealed by a tint etchant (containing 110 mL H_2O, 12 mL H_2SO_4, 4 mL HF and 0,1 mL HNO_3) used at 70°C. Observation at the optical microscope, under polarized light, allows one to discriminate between recovered grains and recrystallized ones, and to determine the incubation time.

For magnetic characterization, toroids of square cross sections 3 x 3mm were machined from the wire after tensile deformation, in order to avoid macroscopic demagnetizing field. Annealing treatment is directly performed on the toroid.

The toroid is then fitted with a primary coil of n_1 turns to which the magnetizing current is fed and with a secondary coil of n_2 turns. Excitation field is measured via V1 using Ampere's theorem, and induction is obtained by numerical integration of the voltage V2 induced by the flux change (Faraday law) [Geoffoy]. The samples were driven through hysteresis cycles at frequencies from 0.1 to 400 Hz for peak induction around 1 T, using the apparatus presented Figure 2.

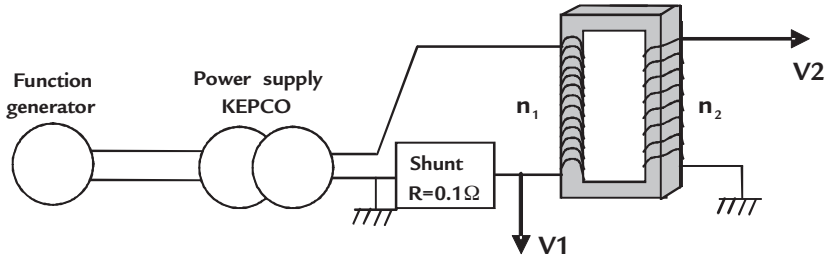

Figure 2
Scheme of the fluxmetric measurement system.

3. Results

Softening kinetics

Evolution of hardness for different annealing time at 750 and 850°C is shown in Figure 3, for both grades. At 750°C, only recovery occurs. At 850°C, incubation time for recrystallization is represented by the arrow. The kinetics of both grades are very similar at 750°C when recovery is the only process involved, but show significant differences at 850°C when recrystallization takes place.

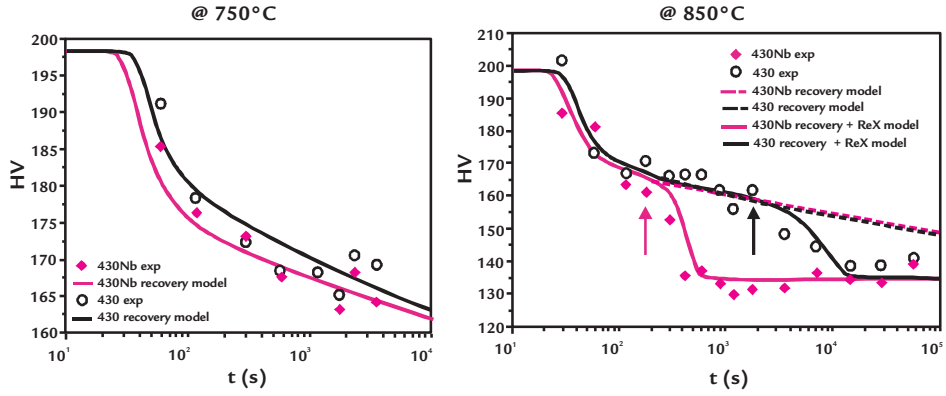

Figure 3
Softening kinetics at 750°C and 850°C determined experimentally. Recovery data (before the arrow) is fitted by Verdier's model with a good agreement [Verdier].

Recrystallization

Recrystallization is much slower in 430 than in 430Nb:

- The onset is considerably delayed for 430. At 850°C, recrystallization starts after 3 min for 430Nb and after 30min for 430.
- A 'sluggish' recrystallization behavior is noted for 430: even 16 h after the onset of recrystallization, deformed grains are still visible. These grains will be called 'island grains' because they are surrounded by recrystallized areas. For 430Nb, recrystallization is complete after 10 min and no 'island grain' is seen.

From a microstructural point of vue, recrystallization leads for both grades to a large increase in the grain size (from 25 µm to about 200 µm) but the morphology of recrystallized grain are clearly different (see Figure 4). In 430Nb, rather equiaxe grains are formed during recrystallization whereas in 430 they have odd shapes with elongated branches.

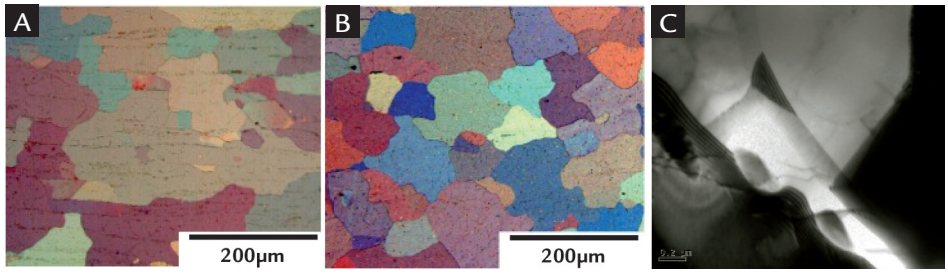

Figure 4
Optical micrographs of 430 and 430Nb after advanced recrystallization (A: 430 after 8 h at 850°C B: 430Nb after 15 min at 850°C) C: TEM image showing interaction between intergranular precipitates and the grain boundary.

Losses

Volumic energy loss per cycle is given by the area of the hysteresis loop B(H). One can notice from Figure 5a, that dissipation at given peak induction is rate dependent and increases when magnetization frequency increases. However losses are also microstructure dependent, as presented Figure 5b. Two largely different microstructures were selected:

430Nb in the deformed state and 430Nb after complete recrystallization (30 min at 850°C). At low frequency, the recrystallized microstructure is more efficient to limit losses, whereas above 550 Hz, the deformed state will be preferred. As a consequence, the frequency is a significant parameter to take into account for microstructure design.

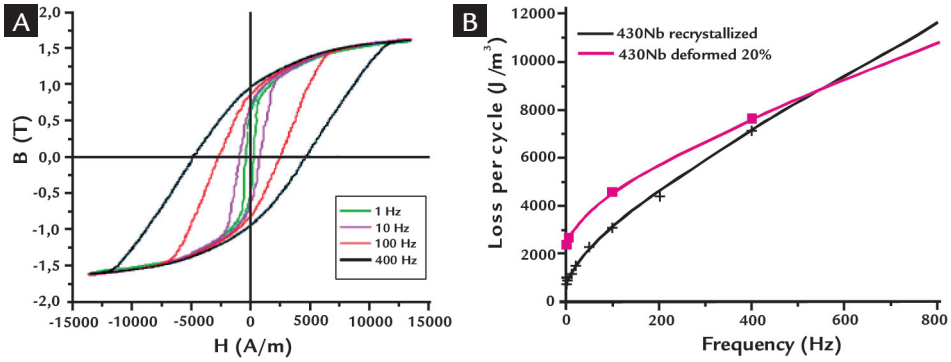

Figure 5
A) Hysteresis loops for 430Nb in recrystallized state at different magnetization frequency and B_{max}=1.6 T. B) Evolution of losses per cycle with frequency for two microstructures at B_{max}=1T; experimental points were fitted by a classical law of the form: $P=A+bf+c\sqrt{f}$ [Geoffroy].

4. Discussion

Recovery model

Before the onset of recrystallization, the softening kinetics were described by the dislocation based model of recovery, developed by Verdier et al. [Verdier]. In this model, the kinetic equation for dislocation density ρ decrease is given by Eq. 1 in which, b is the Burgers vector modulus, E(T) and μ(T) [Rouby] are temperature dependent Young's modulus and shear modulus, M is the Taylor factor, α the interaction coefficient, ν_D the Debye frequency, k the Boltzmann constant, U_0 and ν are activation energy and volume.

$$\frac{d\rho}{dt} = -\frac{4\, b\, E(T)\, \upsilon_D}{M^2\, \alpha\, \mu\,(T(t))}\ \rho^{3/2} \exp\left(-\frac{U_0}{k\,T(t)}\right) \sinh\left(\frac{M\,\alpha\,\mu\,(T(t))\, b\,\sqrt{\rho}\,\upsilon}{k\,T(t)}\right) \quad (1)$$

Eq. 1 was numerically solved under nonisothermal conditions, using the T(t) relationship determined experimentally, that takes into account sample heating stage.

Calibration of the model through activation parameters was done on hardness measurement before the recrystallization onset (see Figure 3). In this attempt, the hardness measurements were related to corresponding dislocation densities via the Taylor law. This work-hardening law is known to be valid for BCC iron at room temperature [Rauch] and was assumed to remain valid for BCC stainless steels. Finally, activation parameters of Eq. 1 were adjusted on the corresponding dislocation densities with a Levenberg-Marquardt optimization method. Good correlation was obtained with the following parameters:

- For 430: U_0 = 330 KJ.mol^{-1} and ν = 49 b^3
- For 430Nb: U_0 = 360 KJ.mol^{-1} and ν = 66 b^3

Activation energies are found to be rather close to self diffusion activation energy Q = 215 KJ.mol^{-1} [Ray], leading to the conclusion that diffusive processes are involved during recovery.

To conclude, it can be noticed from Figure 3 that the model gives an accurate description of the softening kinetics for short time treatments (< 2 min) that are strongly nonisothermal as well as for long time treatment (> 5 min) for which the logarithmic decrease of hardness (HV) is clearly noticed.

Comments on recrystallization

Delay in recrystallization onset as well as 'sluggish' behaviour noticed in 430 (when compared to 430Nb) can both be considered as an effect of the precipitates location.

It is quite well settled that for an IF steel after a low cold deformation, bulging on an existing grain boundary (SIBM) is the prevailing nucleation mechanism [Réglé]. Nucleation occurs if the free length for bulging is larger than the critical radius r* to overcome capillarity effects; r* has an inverse dependence with the pressure ΔP acting on the grain boundary.

Two cases can be distinguished, depending on the distance between precipitates Λ along the boundary:

- If few precipitates are in the grain boundary Λ>>2r*, the free length for bulging is then the subgrain size d_{sg} [Dunlop].
- If intense precipitation takes place in the grain boundary, the free length for bulging is given by the minimum between d_{sg} and Λ.

In the latter description, the three characteristic lengths Λ, d_{sg} and r* are increasing during annealing but at different rates, respectively imposed by the stored energy decrease in each grain due to recovery, subgrain growth and precipitates coarsening.

TEM characterizations, not presented here, gave us some evidence that for 430Nb, Λ>>2r* and nucleation is imposed by subgrain growth, whereas for 430, Λ<d_{sg}, leading to a nucleation imposed by precipitates coarsening.

When precipitates are interacting with SIBM, the first nucleation is followed by growth in the deformed grain, but as soon as another grain boundary is reached, a re-nucleation criterion has to be fulfilled again for growth to continue (the critical size for re-nucleation is expected to be lower than for the first nucleation step because the pressure on the boundary is higher [Bate]). As a consequence of re-nucleation, growth direction will be highly anisotropic leading to odd shapes for recrystallized grains, as observed for 430. In this approach 'island grains' are deformed grains for which the distance between precipitates all around the boundary is too small for re-nucleation to occur.

Comments on magnetic losses

Losses are often considered as a sum of three contributions: $P=P_{hyst}+P_{cl}+P_{ex}$. The classical eddy-current energy losses per cycle (P_{cl}) depend on geometry, peak induction, resistivity and frequency, whereas the two other contributions hysteresis losses (P_{hyst}) and excess losses (P_{ex}) are in addition microstructure dependent. P_{hyst} represents the total losses under quasistatic conditions and features the same microstructure dependence than coercive field Hc. In other words, defects experienced by a moving domain-wall are responsible of the macroscopic counter field Hc as well as the resulting energy dissipation P_{hyst}. Excess losses term is due to the spatial distribution of eddy-currents associated to domain walls displacements, strongly different from the distribution associated to classical approximation. Depending on microstructure, moving walls are considered as independent (case of GOSS textured materials) or as global "Magnetic Objects" (MOs) if strongly correlated (case of materials investigated here). The amplitude of excess losses is strongly related to the number of moving MOs, this parameter depending on microstructure too.

Grain size d is the main microstructural parameter whose effect has been studied for both contributions. Hysteresis losses term decreases as 1/d whereas excess losses increases as $\sqrt{d.f}$ leading to an optimum grain size depending on frequency f [Campos].

For 430Nb, recrystallization leads to a large increase of grain size. Considering only this microstructural aspect, the detrimental effect of recrystallization on magnetic losses, noticed experimentally at high frequency, can be well understood.

5. Conclusions

Niobium stabilization is changing completely the precipitates location from intergranular to homogeneous distribution. No effects were found on recovery kinetics, although, for higher Nb stabilization level, such an effect was already reported in the literature [Mantel]. However, low Nb stabilization greatly facilitates recrystallization process: the incubation time for recrystallization is significantly lowered and the 'sluggish' behaviour is avoided. A SIBM nucleation in interaction with precipitates can explain qualitatively these differences in softening kinetics, as well as the difference in grain morphology. A quantitative model has been proposed to describe recrystallization for both grades.

Moreover, magnetic losses have been shown to be microstructure sensitive. This dependence concerns two contributions: P_{hyst} and P_{exc}. Looking to the effect of grains size, one notices opposite effects in each contribution, leading to an optimum size. If grain size effect is extensively described in literature dislocations and misorientation between grains, effects on magnetic losses have not been much studied. Recovered states will be considered for this purpose.

6. Acknowledgement

Many thanks to E. Rauch, M. Verdier, D. Gex and F. Robaut for their help and stimulating discussions. The authors gratefully acknowledge Mariana Perez de Oliveira from CBMM for funding this study.

7. References

ARA, K. Magnetic characteristics of ferromagnetic stainless steels. ***IEEE Transactions on Magnetics***, v. 25, n.3, p. 2617-2623, 1989.

BATE P., HUTCHINSON, B. A re-evaluation of the mechanism of SIBM. ***Scripta Materialia***, v. 36, Issue 2, p. 195-198, January 1997.

CAMPOS, M.F., YONAMINE, T., FUKUHARA, M., LANDGRAF, F.J.G., ACHETE, C.A., MISSELL, F.P. Effect of frequency on the iron losses of 0.5% and 1.5% Si nonoriented electrical steels. ***IEEE Transactions on Magnetics***, v. 42, n. 10, p.2812-2814, 2006.

GEOFFROY, O. Physique des matériaux magnétiques. In: ***Techniques de l'Ingénieur.*** In: T.I. Sciences et Techniques (Ed.), v. D2080, 2006.

MANTEL, M., BAROUX, B., GEX, D. AND PEDARRE, P. ***Recrystallization '90***, edited by T. Chandra, The Minerals, Metals & Materials Society, p. 345, 1990.

RAUCH E. ***Etude de l'écrouissage des métaux : aspects microstructuraux et lois de comportement***. Thesis, Institut National Polytechnique de Grenoble, 1993.

RAY, S.P., SHARMA, B.D. Diffusion of Fe^{59} in Fe-Cr alloys. ***Acta Metallurgica***, v. 16, issue 8, p. 981-986, 1968.

REGLE, H., HDR Thesis Université Paris 13, 2005.

ROUBY, M., BLANCHARD, P. Propriétés physiques et mécanique des aciers et alliages inoxydables. In: LACOMBE, P. (Ed.). p.109, Chapter 4 in Les aciers inoxydables, EDP, 1990.

VERDIER, M., BRÉCHET, Y. , GUYOT, P. Recovery of AlMg alloys: flow stress and strain-hardening properties. ***Acta. Mater.***, v. 47, p.127-134, 1999.

Paper submitted to INOX 2010- 10th Brazilian Stainless Steel Conference, September 20-22, Rio de Janeiro, Brazil. Revised accepted December, 28, 2012.